SINGLE IMAGE SUPER-RESOLUTION VIA AN ITERATIVE REPRODUCING KERNEL HILBERT SPACE METHOD

LIANG-JIAN DENG*, WEIHONG GUO†, AND TING-ZHU HUANG‡

Abstract. Image super-resolution, a process to enhance image resolution, has important applications in satellite imaging, high definition television, medical imaging, etc. Many existing approaches use multiple low-resolution images to recover one high-resolution image. In this paper, we present a thin-plate spline based iterative reproducing kernel Hilbert space (RKHS) method to solve *single* image super-resolution problems. It recovers a high quality high-resolution image from solely one low-resolution image. The iterative RKHS method has a *closed-form* solution and the algorithm parameters are easy to select. Visual and quantitative comparisons show that the proposed method can recover more accurate details. Especially, the proposed method overcomes the jaggy effect of nearest-neighbor interpolation and reduces the blur effect of bicubic interpolation significantly. The proposed method can also get comparable results with two state-of-the-art learning-based methods that need a lot of training data.

Key words. Image super-resolution, Iterative RKHS, Closed-form solution, Thin-plate spline

AMS subject classifications.

1. Introduction.

Image super-resolution (SR), a quite active research field currently, is a process to estimate a high-resolution (HR) image from one or multiple low-resolution (LR) images. High-resolution means more details and better visibility. Due to limitation of hardware devices and high cost, one sometimes only can collect low-resolution images. For instance, synthetic aperture radar (SAR) and satellite imaging can not get high-resolution images due to long distance and air turbulence. In medical imaging MRI, high-resolution images need more time and cost [50, 38]. Thus, developing a more accurate and faster image super-resolution algorithm is important and has a lot of applications.

1.1. Literature review.

In this section we review some existing super-resolution methods, some of which will be compared with the proposed method.

Many existing image super-resolution methods need multiple low-resolution images as inputs. We refer to them as multiple image super-resolution. Mathematically, there are p low-resolution images $y_i \in \mathbb{R}^m$ available, y_i is related to a high-resolution image $x \in \mathbb{R}^n$ by

$$y_i = DB_i x + n_i, 1 \leq i \leq p, \tag{1.1}$$

where $D \in \mathbb{R}^{m\times n}$ is a down-sampling operator and $B_i \in \mathbb{R}^{n\times n}$ is a blurring operator that might happen due to for instance out of focus, $n_i \in \mathbb{R}^m$ represents random noise [42].

This paper addresses single image super-resolution, i.e., $p = 1$ in equation (1.1). Compared to multiple image super-resolution, single image super-resolution is more useful as one normally only has one low-resolution image available. Obviously, it is also more challenging.

Existing image super-resolution methods can be divided into several categories: interpolation-based methods, statistics-based methods, learning-based approaches and others (e.g., frequency techniques, pixel classification methods, etc). Note that, these methods are not completely independent. For example, some of the learning-based methods may belong to the category of statistics-based methods.

Interpolation is a straightforward idea for image super-resolution. There are two popular interpolation methods: nearest-neighbor interpolation and bicubic interpolation. Nearest-neighbor interpolation fills in intensity at an unknown location by that of its nearest neighbor point. It often causes jaggy effect (see the right image in Figure 1). Bicubic interpolation is

*School of Mathematical Sciences, University of Electronic Science and Technology of China, Chengdu, Sichuan, 611731, P. R. China. (liangjian1987112@126.com).

†The Corresponding Author. Department of Mathematics, Case Western Reserve University, Cleveland, OH, 44106, USA. (wxg49@case.edu).

‡School of Mathematical Sciences, University of Electronic Science and Technology of China, Chengdu, Sichuan, 611731, P. R. China. (tingzhuhuang@126.com).

FIG. 1. *Left one is a low-resolution image; middle image is the super-resolution image using bicubic interpolation method (note the blurry effect); right one is the super-resolution image by nearest-neighbor interpolation method (note the jaggy effect on the edges); upscaling factor is 4.*

to utilize a cubic kernel to interpolate. It tends to create blur effect (see the middle image in Figure 1).

Maximum a Posterior (MAP) and Maximum Likelihood estimator (MLE) are popular statistics-based methods [18, 6, 19]. To preserve sharp edges, Fattal [19] utilized statistical edge dependency to relate edge features in low and high resolution images. Farsin et al. [18] proposed an alternate approach using L_1 norm minimization and a bilateral prior based robust regularization.

Learning-based approaches are a powerful tool for image super-resolution [24, 23, 45, 49, 25, 22, 44, 30, 29, 32, 60, 54, 47, 9, 20]. They normally start from two large training data sets, one formed of low-resolution images and the other formed of high-resolution images, and then learn a relation between low-resolution and high-resolution images. The relation is then applied to a given low-resolution image to get a high-resolution image. The results depend on the selection of training data. Learning-based methods usually can obtain high quality images but they are computationally expensive. Additionally, they are not a completely single image super-resolution since two large data sets are required for learning. In [45], Sun et al. utilized sketch priors to extend the low vision learning approach in [24] to get clear edges, ridges and corners. Sun et al. in [44] proposed a novel profile prior of image gradient which can describe the shape and the sharpness of an image to obtain super-resolution images. Xie et al. proposed a method via an example-based strategy which divides the high-frequency patches of a low-resolution image into different classes [54]. This method can accelerate image super-resolution procedure. Fernandez-Granda and Candès used transform-invariant group-sparse regularization [20]. This method performs well for highly structured straight edges and high upscaling factors. In recent years, sparsity methods, usually associated with learning-based ideas, have been widely discussed for image super-resolution [57, 56, 55, 59, 26, 14, 58]. In [57, 56], Yang et al. utilized sparse signal representation to develop a novel method for single image super-resolution. The authors first sought a sparse representation for each patch of the low-resolution image and computed corresponding coefficients, then generated the high-resolution image via the computed coefficients. Recently, Zeyde and Elad et al. [58] proposed a local sparse-land model on image patches based on the work of [57, 56], and obtained improved results.

In addition, many other image super-resolution methods also have been proposed, e.g., a frequency technique [3], pixel classification methods [1, 2], iterative back projection methods [27, 31, 10, 46], a hybrid method [13], a kernel regression method [48] and others [51, 5, 21].

In summary, single image super-resolution is still a challenging problem. Existing single image super-resolution methods either need training data sets and expensive computation or lead to blur or jaggy effect. The aim of this paper is to use a simple mathematical scheme to recover a high quality high-resolution images for one low-resolution image.

1.2. Motivation and contributions of the proposed work. In this paper, we plan to use RKHS method to study single image super-resolution with only one low-resolution image

as an input. We cast the super-resolution problem as an image intensity function estimation problem. We assume that the intensity function f belongs to a special Hilbert space called RKHS that can be spanned by a basis. We use intensities information of the given low-resolution image defined on a coarse grid to estimate basis coefficients, and then utilize the coefficients to generate high-resolution images at any fine grids. We will use thin-plate spline based RKHS which has been used for smoothing problems in [52], one can apply the same model in [52] for image super-resolution but it may cause blur. To overcome the blur effect, we propose an iterative RKHS method based on thin-plate spline for single image super-resolution, aiming to recover more sharp details. The iterative RKHS method is inspired by the iterative back projection method in [27] and the iterative regularization method in [37].

This paper has the following main contributions:

- To the best of our knowledge, this is the first work to employ RKHS method to get competitive image super-resolution results. RKHS-based methods have been considered as a powerful tool to address machine learning for a long time. In image processing, however, only limited studies have been done, e.g., image denoising [4], image segmentation [28] and image colorization [39].
- *Single* image super-resolution. The proposed method only needs one low-resolution image as an input. Competitive learning-based methods actually need to train two large data sets, one formed of low-resolution images and the other formed of high-resolution images, to find a relation between the low-resolution and high-resolution images.
- Simplicity and flexibility. The proposed RKHS model has a very simple formulation. It has a *closed-form solution*. The parameter selection and upscaling factors are flexible. Parameter selection is not sensitive and one can choose any integer or fraction upscaling factors.

1.3. Organization of this paper. The organization of this paper is as follows. In Section 2, we review RKHS and splines based RKHS. We will also give three remarks in this section. In Section 3, we proposed an iterative RKHS model for single image super-resolution, and give a closed-form solution of the proposed model. Many visual and quantitative experiments are shown in Section 4 to demonstrate the proposed method is a competitive approach for single image super-resolution. Finally, we draw conclusions in Section 5.

2. Review on splines based RKHS. In this section, we review RKHS, splines based RKHS in [52] and their applications in signal/image smoothing.

2.1. Review on RKHS and its applications. Given a subset $\mathcal{X} \subset \mathbb{R}$ and a probability measure $\mathbb{P}$ on $\mathcal{X}$, we consider a Hilbert space $\mathcal{H} \subset L^2(\mathbb{P})$, a family of functions $g : \mathcal{X} \to \mathbb{R}$, with $\|g\|_{L^2(\mathbb{P})} < \infty$, and an associated inner product $\langle \cdot, \cdot \rangle_{\mathcal{H}}$ under which $\mathcal{H}$ is complete. The space $\mathcal{H}$ is a reproducing kernel Hilbert space (RKHS), if there exists a symmetric function $\mathbb{K} : \mathcal{X} \times \mathcal{X} \to \mathbb{R}$ such that: (a) for each $x \in \mathcal{X}$, the function $\mathbb{K}(\cdot, x)$ belongs to Hilbert space $\mathcal{H}$, and (b) there exists reproducing relation $f(x) = \langle f, \mathbb{K}(\cdot, x) \rangle_{\mathcal{H}}$ for all $f \in \mathcal{H}$. Any such symmetric kernel function must be positive semidefinite (see Definition 2.1). Under suitable regularity conditions, Mercer's theorem [34] guarantees that the kernel has an eigen-expansion of the form $\mathbb{K}(x, x') = \sum_{k=1}^{\infty} \lambda_k \phi_k(x) \phi_k(x')$, with $\lambda_1 \geq \lambda_2 \geq \lambda_3 \geq \ldots \geq 0$ being a non-negative sequence of eigenvalues, and $\{\phi_k\}_{k=1}^{\infty}$ associated eigenfunctions, taken to be orthonormal in $L^2(\mathbb{P})$.

DEFINITION 2.1. *(Positive Semidefinite Kernel) Let $\mathcal{X}$ be a nonempty set. The kernel $\mathbb{K} : \mathcal{X} \times \mathcal{X} \to \mathbb{R}$ is positive semidefinite if and only if Gram matrix $K = [\mathbb{K}(x_i, x_j)]_{N \times N}$, $x_i \in \mathcal{X}, i, j = 1, 2, \cdots, N$, is a positive semidefinite matrix.*

Since the eigenfunctions $\{\phi_k\}_{k=1}^{\infty}$ form an orthonormal basis, any function $f \in \mathcal{H}$ has an expansion of the form $f(x) = \sum_{k=1}^{\infty} \sqrt{\lambda_k} a_k \phi_k(x)$, where $a_k = \langle f, \phi_k \rangle_{L^2(\mathbb{P})} = \int_{\mathcal{X}} f(x) \phi_k(x) \, d\mathbb{P}(x)$ are (generalized) Fourier coefficients. Associated with any two functions in $\mathcal{H}$, where $f = \sum_{k \geq 1} \sqrt{\lambda_k} a_k \phi_k$ and $g = \sum_{k \geq 1} \sqrt{\lambda_k} b_k \phi_k$, are two distinct inner products. The first is the usual inner product in the space $L^2(\mathbb{P})$ defined as $\langle f, g \rangle_{L^2(\mathbb{P})} := \int_{\mathcal{X}} f(x) g(x) \, d\mathbb{P}(x) = \sum_{k=1}^{\infty} \lambda_k a_k b_k$. by Parseval's theorem. The second inner product, denoted $\langle f, g \rangle_{\mathcal{H}}$, defines the Hilbert space. It can be written

in terms of the kernel eigenvalues and generalized Fourier coefficients as $\langle f, g\rangle_{\mathcal{H}} = \sum_{k=1}^{\infty} a_k b_k$. Using this definition, the Hilbert ball of radius 1 for $\mathcal{H}$ with eigenvalues λ_k and eigenfunctions $\phi_k(\cdot)$, is $\mathbb{B}_{\mathcal{H}}(1) = \{f \in \mathcal{H};\ f(\cdot) = \sum_{k=1}^{\infty} \sqrt{\lambda_k} b_k \phi_k(\cdot) \mid \sum_{k=1}^{\infty} b_k^2 = \|b\|_2^2 \leq 1\}$. The class of RKHS contains many interesting classes that are widely used in practice including polynomials of degree d ($\mathbb{K}(x, y) = (1 + \langle x, y\rangle)^d$), Sobolev spaces with smoothness ν, Lipschitz, and smoothing splines. Moreover, kernel $\mathbb{K}(x, x') = \frac{1}{2} e^{-\gamma|x-x'|}$ leads to Sobolev space $\mathcal{H}_1$, i.e., a space consisted of square integrable functions whose first order derivative is square integrable. $\mathbb{K}(x, x') \propto |x - x'|, \mathbb{K}(x, x') \propto |x - x'|^3$ correspond to 1D piecewise linear and cubic splines respectively.

RKHS has appeared for many years, and it has been used as a powerful tool for machine learning [52, 36, 40, 43, 11, 7, 8, 35, 12]. Its application in image processing is not so common yet. In [4], Bouboulis et al. proposed an adaptive kernel method to deal with image denoising problem in the spatial domain. This method can remove many kinds of noise (e.g., Gaussian noise, impulse noise, mixed noise) and preserves image edges effectively. In addition, Kang et al. utilized RKHS method to do image segmentation [28] and image/video colorization [39].

Wahba proposed splines based RKHS for smoothing problems in [52]. It shows that the solution of an optimization problem consists of a set of polynomial splines. The proposed method is based on splines based RKHS. We thus review them in the following two subsections.

2.2. A 1D spline and signal smoothing. For a real-valued function $f \in \mathcal{G} = \{f : f \in \mathcal{C}^{m-1}[0, 1], f^{(m)} \in \mathcal{L}_2[0, 1]\}$, it can be expanded at $t = 0$ by Taylor series as:

$$f(t) = \sum_{\nu=0}^{m-1} \frac{t^\nu}{\nu!} f^{(\nu)}(0) + \int_0^1 \frac{(t-u)_+^{m-1}}{(m-1)!} f^{(m)}(u)du = f_0(t) + f_1(t), \tag{2.1}$$

with $f_0(t) = \sum_{\nu=0}^{m-1} \frac{t^\nu}{\nu!} f^{(\nu)}(0)$ and $f_1(t) = \int_0^1 \frac{(t-u)_+^{m-1}}{(m-1)!} f^{(m)}(u)du$, where $(u)_+ = u$ for $u \geq 0$ and $(u)_+ = 0$ otherwise.

Let $\phi_\nu(t) = \frac{t^{\nu-1}}{(\nu-1)!}, \nu = 1, 2, ..., m$, $\mathcal{H}_0 = \text{span}\{\phi_1, \phi_2, ..., \phi_m\}$ with norm $\|\phi\|^2 = \sum_{\nu=0}^{m-1} [(D^{(\nu)}\phi)(0)]^2$, then $D^{(m)}(\mathcal{H}_0) = 0$. It has been proved in [52] that $\mathcal{H}_0$ is a RKHS with reproducing kernel $R^0(s, t) = \sum_{\nu=1}^{m} \phi_\nu(s)\phi_\nu(t)$. For a function $f_0 \in \mathcal{H}_0$, we can express f_0 using the basis of $\mathcal{H}_0$, i.e., $f_0(t) = \sum_{\nu=1}^{m} d_\nu \phi_\nu(t)$.

Let $\mathcal{B}_m$ be a set of functions satisfying boundary condition $f^{(\nu)}(0) = 0, \nu = 0, 1, 2, \cdots, m-1$ and $G_m(t, u) = \frac{(t-u)_+^{m-1}}{(m-1)!}$, then $f_1(t) = \int_0^1 \frac{(t-u)_+^{m-1}}{(m-1)!} f^{(m)}(u)du = \int_0^1 G_m(t, u) f^{(m)}(u)du$ belongs to space $\mathcal{H}_1$ defined as follows

$$\mathcal{H}_1 = \{f : f \in \mathcal{B}_m, f, f', ..., f^{(m-1)} \text{absolutely continuous}, f^{(m)} \in \mathcal{L}_2\}, \tag{2.2}$$

where $\mathcal{H}_1$ is a Hilbert space on [0,1] with norm $\|f\|^2 = \int_0^1 (f^{(m)}(t))^2 dt$. $\mathcal{H}_1$ also has been proved to be a RKHS in [52] with reproducing kernel $R^1(s, t) = \int_0^1 G_m(t, u)G_m(s, u)du$. For a function $f_1 \in \mathcal{H}_1$, we can express f_1 via the basis of $\mathcal{H}_1$, denoted by $\{\xi_i\}_{i=1}^n$, so that $f_1(t) = \sum_{i=1}^n c_i \xi_i(t) = \sum_{i=1}^n c_i R^1(s_i, t)$, where $\xi_i = R^1(s_i, \cdot)$.

Due to $\int_0^1 ((D^{(m)} f_0)(u))^2 du = 0$ and $\sum_{\nu=0}^{m-1} ((D^{(\nu)} f_1)(0))^2 = 0$, we can construct a direct sum space $\mathcal{G}_m$ by the two RKHS spaces $\mathcal{H}_0$ and $\mathcal{H}_1$, i.e., $\mathcal{G}_m = \mathcal{H}_0 \oplus \mathcal{H}_1$. $\mathcal{G}_m$ is proved as a RKHS in [52] with the following reproducing kernel

$$R(s, t) = \sum_{\nu=1}^{m} \phi_\nu(s)\phi_\nu(t) + \int_0^1 G_m(t, u)G_m(s, u)du, \tag{2.3}$$

and norm

$$\|f\|^2 = \sum_{\nu=0}^{m-1} [(D^{(\nu)} f)(0)]^2 + \int_0^1 (f^{(m)})^2(t)dt, \tag{2.4}$$

where $f \in \mathcal{G}_m$. As a summary, for $f \in \mathcal{G}_m$, we have $f = f_0 + f_1$, with $f_0 \in \mathcal{H}_0$, $f_1 \in \mathcal{H}_1$. It also can be written as

$$f(t) = \sum_{\nu=1}^{m} d_\nu \phi_\nu(t) + \sum_{i=1}^{n} c_i \xi_i(t), \tag{2.5}$$

where $t \in [0, 1]$.

let $\vec{f} = (f(t_1), f(t_1), \cdots, f(t_n))'$ be intensity values of f at $t_i \in [0, 1], i = 1, 2, \cdots, n$, let

$$\vec{g} = \vec{f} + \eta, \tag{2.6}$$

be a noisy observation with η an additive Gaussian noise.

Let T be a $n \times m$ matrix with $T_{i,\nu} = \phi_\nu(t_i)$ and let Σ be a $n \times n$ matrix with $\Sigma_{i,j} =< \xi_i, \xi_j >$, we have the relation $\vec{f} = Td + \Sigma c$ where $d = (d_1, d_2, \cdots, d_m)'$ and $c = (c_1, c_2, \cdots, c_n)'$. In [52], the following model is used to estimate $\vec{f}$ from noisy discrete measurements $\vec{g}$,

$$\min_{c,d} \frac{1}{n} \|\vec{g} - Td - \Sigma c\|^2 + \lambda c' \Sigma c, \tag{2.7}$$

where the second term penalties nonsmoothness.

The simple model (2.7) has a closed-form solution: $d = (T'M^{-1}T)^{-1}T'M^{-1}\vec{g}$, $c = M^{-1}(I - T(T'M^{-1}T)^{-1}T'M^{-1})\vec{g}$ where $M = \Sigma + n\lambda I$ with I an identity matrix. The computation burden of matrix inverse can be reduced via QR decomposition (see details in Chapter 1 of [52]).

Remark 1 Once c and d are estimated from equation (2.7), one can get an estimate for the signal function $f(x)$,

$$f(x) = \sum_{\nu=1}^{m} d_\nu \phi_\nu(x) + \sum_{i=1}^{n} c_i \xi_i(x) = \sum_{\nu=1}^{m} d_\nu \phi_\nu(x) + \sum_{i=1}^{n} c_i R^1(s_i, x), \tag{2.8}$$

for any $x \in [0, 1]$.

Next, we will review 2D thin-plate spline which can be viewed as an extension of the mentioned 1D spline.

2.3. 2D thin-plate spline and image smoothing. We use 2D thin-plate spline based RKHS, introduced in [52], for image super-resolution in this paper. We thus review it.

Similar to the 1D case, let f be the intensity function of a 2D image defined on a continuous domain $E^2 = [0, 1] \times [0, 1]$. We assume f belongs in a RKHS. Let $\vec{f} = (f(t_1), f(t_1), \cdots, f(t_n))'$ be its discretization on grids $t_i = (x_i, y_i) \in [0, 1] \times [0, 1], i = 1, 2, \cdots, n$, the noisy image of vector form with an additive noise η can be described by

$$\vec{g} = \vec{f} + \eta. \tag{2.9}$$

In [52], an optimal estimate of f for spline smoothing problems can be obtained by minimizing the following model

$$\min \frac{1}{n} \|\vec{g} - \vec{f}\|^2 + \lambda J_m(f), \tag{2.10}$$

where m is a parameter to control the total degree of polynomial, and the penalty term is defined as follows

$$J_m(f) = \sum_{\nu=0}^{m} \int_{-\infty}^{+\infty} \int_{-\infty}^{+\infty} C_m^\nu \left(\frac{\partial^m f}{\partial x^\nu \partial y^{m-\nu}}\right)^2 dxdy, \tag{2.11}$$

From Chapter 2 of [52], we know that the null space of the penalty function $J_m(f)$ is a $M = C_{d+m-1}^d$ dimension space spanned by the polynomials of degree no more than $m - 1$. In

the experiments, we let $d = 2$ (for 2D), $m = 3$, then $M = C_{d+m-1}^{d} = 6$, so the null space can be spanned by the following terms: $\phi_1(x, y) = 1, \phi_2(x, y) = x, \phi_3(x, y) = y, \phi_4(x, y) = xy, \phi_5(x, y) = x^2, \phi_6(x, y) = y^2$. Duchon (see [17]) has proved that if there exists $\{t_i\}_{i=1}^{n}$ so that least squares regression on $\{\phi_\nu\}_{\nu=1}^{M}$ is unique, then the optimization model (2.10) has a unique solution as follows

$$f_\lambda(t) = \sum_{\nu=1}^{M} d_\nu \phi_\nu(t) + \sum_{i=1}^{n} c_i E_m(t, t_i), \tag{2.12}$$

where $E_m(t, t_i)$ is a Green's function for the m-iterated Laplacian defined as:

$$E_m(s, t) = E_m(|s - t|) = \theta_{m,d}|s - t|^{2m-d}\ln|s - t|,$$

where $\theta_{m,d} = \frac{(-1)^{d/2+m+1}}{2^{2m-1}\pi^{d/2}(m-1)!(m-d/2)!}$, especially, $E_m(t, t_i)$ plays the same role with $\xi_i(t)$ in 1D case.

Similar with equation (2.7), model (2.10) can be rewritten as:

$$\min \frac{1}{n}\|\vec{g} - (Td + Kc)\|^2 + \lambda c' K c, \tag{2.13}$$

where T is a $n \times M$ matrix with $T_{i,\nu} = \phi_\nu(t_i)$ and K is a $n \times n$ matrix with $K_{i,j} = E_m(t_i, t_j)$. This model also has a similar closed-form solution with 1D case: $d = (T'W^{-1}T)^{-1}T'W^{-1}\vec{g}$, $c = W^{-1}(I - T(T'W^{-1}T)^{-1}T'W^{-1})\vec{g}$ where $W = K + n\lambda I$. Additionally, a more economical version that utilizing QR decomposition also has been provided to compute the coefficients c and d (see details in [52]). Moreover, more information about the thin-plate spline can also be found in [15, 16, 17, 33, 53, 41].

Remark 2 Once we have computed coefficients c and d, the underlying function f on the continuous domain E^2 can be estimated as

$$f(w) = \sum_{\nu=1}^{M} d_\nu \phi_\nu(w) + \sum_{i=1}^{n} c_i E_m(t_i, w), \tag{2.14}$$

for any $w = (x, y)' \in E^2$. One thus can get an estimate of $f(w)$ at any $w \in [0, 1] \times [0, 1]$. This is very powerful and makes image super-resolution possible.

In particular, one can evaluate f on fine grids to get super-resolution images.

Remark 3 *Let $\widetilde{T} \in \mathbb{R}^{N\times M}$ and $\widetilde{K} \in \mathbb{R}^{N\times n}$ be defined similarly with $T \in \mathbb{R}^{n\times M}$ and $K \in \mathbb{R}^{n\times n}$, where n, N are the grid numbers on coarse grids and fine grids, respectively; c and d are computed in model (2.13), then the discrete signal $\tilde{f}$ on fine grids can be represented as follows*

$$\tilde{f} = \widetilde{T}d + \widetilde{K}c = \left(\widetilde{T}(T'W^{-1}T)^{-1}T'W^{-1} + \widetilde{K}W^{-1}(I - T(T'W^{-1}T)^{-1}T'W^{-1})\right)\vec{g}, \tag{2.15}$$

where $W = K + n\lambda I$, $\vec{g}$ is the discrete signal on a coarse grid.

Since model (2.13) is for image smoothing, super-resolution result (2.15) sometimes tends to be smooth. In what follows, we present a thin-plate spline based iterative RKHS method to recover high quality high-resolution images with details.

3. The proposed iterative RKHS method. Let f represent intensity function of an image defined on a continuous domain $E^2 = [0, 1] \times [0, 1]$. Let H, L be a high-resolution and a low-resolution discretization of f, respectively. For notation simplicity, we interchangeably use H, L to represent their matrix and vector representations. H and L are usually formulated by $L = DBH + \epsilon$ described in equation (1.1), with D, B a down-sampling and a blurring operator, respectively, ϵ some random noise or 0 for noise-free case. We note that high-resolution image $H \in \mathbb{R}^{U\times V}$ can be obtained by $H_i = f(t_i^h)$ with $t_i^h = (x_i, y_i)$, $x_i \in \{0, \frac{1}{U-1}, \frac{2}{U-1}, \cdots, 1\}$, $y_i \in \{0, \frac{1}{V-1}, \frac{2}{V-1}, \cdots, 1\}$ on a fine grid. Low-resolution image $L \in \mathbb{R}^{Q\times S}$ is gotten by the discretization formula $L_i = f(t_i^l)$ with $t_i^l = (x_i, y_i)$, $x_i \in \{0, \frac{1}{Q-1}, \frac{2}{Q-1}, \cdots, 1\}$, $y_i \in \{0, \frac{1}{S-1}, \frac{2}{S-1}, \cdots, 1\}$

on a coarse grid. In particular, Q, S are smaller than U, V, respectively. Actually, $T^l \in \mathbb{R}^{n\times M}$, $K^l \in \mathbb{R}^{n\times n}$ and $T^h \in \mathbb{R}^{N\times M}$, $K^h \in \mathbb{R}^{N\times n}$ are the T, K matrices and $\widetilde{T}, \widetilde{K}$ matrices in Section 2.3, respectively, where $n = Q \cdot S$, $N = U \cdot V$ and M is the dimension of the null space of the penalty term (see details also in Section 2.3). Motivated by the smoothing model (2.13), c, d can be solved using the following model

$$\min \frac{1}{n}\|L - DB(T^h d + K^h c)\|^2 + \lambda c' K^l c, \tag{3.1}$$

where $H = T^h d + K^h c$.

Model (3.1) leads to blur results along edges of high-resolution image due to smoothing property of thin-plate spline model (2.13). In particular, we observe residual edges in difference image $L - DBH^{(1)}$ where $H^{(1)}$ is the computed high-resolution image by model (3.1). Inspired by the iterative back projection method [27] and the iterative regularization method [37], we consider the difference $L - DBH^{(1)}$ as a new low-resolution input L, and recompute the model to get a residual high-resolution image $H^{(2)}$. We repeat this process until the residual is small enough. The sum of the high-resolution image $H^{(1)}$ and its residual high-resolution images is the resulted super-resolution image $\widehat{H}$. The strategy can recover more image details. In Figure 2, (c) and (d) show the details $H^{(2)}$ and $H^{(3)}$ recovered at iterate 2 and 3, respectively. One can see that $H^{(3)}$ has no obvious edges. The resulted image (a), $H^{(1)} + H^{(2)} + H^{(3)}$, is sharper than resulted image (b), $H^{(1)}$ that is the result of model (3.1). Instead of adding all $H^{(i)}$ together, one can also do a weighted sum, i.e., $\widehat{H} = \sum_{i=1}^{\tau} \alpha_i H^{(i)}$ where τ is the maximum number of iteration and $\alpha_i \geq 0$. In our experiments, it is enough to iterate the process three times. The following Algorithm 1 is the proposed iterative RKHS algorithm for single image super-resolution. This algorithm can work for general D, B though we mainly tested it with bicubic down-sampling and Gaussian blur in the experiments.

Algorithm 1 (Single image super-resolution via RKHS (SR-RKHS))

Input: one low-resolution image $L \in \mathbb{R}^{Q\times S}$, $\lambda > 0$
τ: maximum number of iteration, $\alpha_i \geq 0, i = 1, 2, \cdots, \tau$.
Output: high-resolution image $\widehat{H} \in \mathbb{R}^{U\times V}$

1. Set coarse grids t^l and fine grids t^h.
2. Construct matrices T^l, K^l using $T^l_{i,\nu} = \phi_\nu(t^l_i)$ and $K^l_{i,j} = E_m(t^l_i, t^l_j)$, $i, j = 1, 2, \cdots, n$, $n = Q.S$, $\nu = 1, 2, \cdots, M$. Similarly for T^h, K^h except $i = 1, 2, \cdots, N; j = 1, 2, \cdots, n$, where $N = U \cdot V$.
3. Initialization: $L^{(1)} = L$.
   for k = 1:τ
   a. Compute the coefficients: $(c^{(k)}, d^{(k)}) = \text{argmin}\frac{1}{n}\|L^{(k)} - DB(T^h d + K^h c)\|^2 + \lambda c' K^l c$.
   b. Update the high-resolution image: $H^{(k)} = T^h d^{(k)} + K^h c^{(k)}$.
   c. Down-sampling $H^{(k)}$ to coarse grid: $\widetilde{L} = DBH^{(k)}$.
   d. Compute residual: $L^{(k+1)} = L^{(k)} - \widetilde{L}$.
   end
4. Compute the final high-resolution image with weighted correction:
$$\widehat{H} = \sum_{i=1}^{\tau} \alpha_i H^{(i)}.$$

Note that although we introduce some parameters in the super-resolution algorithm, these parameters are all not sensitive and easy to select. For example, parameter λ, required as small as possible for noise-free case, is 1×10^{-35} in all experiments. If we choose $\lambda = 10^{-30}$ or $\lambda = 10^{-40}$, the algorithm leads to similar results. The iterative RKHS method needs only a few iterations ($\tau = 3$ in all experiments). In addition, weighting coefficients $\alpha_1 = 1, \alpha_2 = 1, \alpha_3 = 1$ in our experiments.

In this study, we have tested blur-free case ($B = I$), blur case and noise case. For these cases, $DB(T^h d + K^h c)$, in step 3a of Algorithm 1, is always considered as $T^l d + K^l c$ in practice. Then we obtain high-resolution image in step 3b of Algorithm 1 by the computed coefficients in step 3a. Actually, step 3a and step 3b of Algorithm 1 can be replaced by the closed-form

formula (2.15). Down-sampling operators D, associating with step 3a and step 3c in Algorithm 1, are done by bicubic interpolation (In MATLAB function: 'imresize').

Algorithm 1 has a closed-form solution for blur-free case.

THEOREM 3.1. *Let L be the vector form of a low-resolution image and I be an identity matrix, τ is the number of maximum iteration in Algorithm 1, D represents a down-sampling operator, the output of Algorithm 1 is as follows*

$$\widehat{H} = \left(\sum_{i=1}^{\tau} \alpha_i R - \sum_{i=2}^{\tau} \alpha_i RDR - \alpha_i \sum_{i=3}^{\tau} \sum_{j=1}^{i-2} RD(I - RD)^j R \right) L, \tag{3.2}$$

where $R = T^h(T^{l'}W^{-1}T^l)^{-1}T^{l'}W^{-1} + K^hW^{-1}(I - T^l(T^{l'}W^{-1}T^l)^{-1}T^{l'}W^{-1})$, $W = K^l + n\lambda I$, λ is the regularization parameter in model (3.1).

Proof. According to Remark 3, we know that

$$H = T^h d + K^h c,$$

where $c = W^{-1}(I - T^l(T^{l'}W^{-1}T^l)^{-1}T^{l'}W^{-1})L$, $d = (T^{l'}W^{-1}T^l)^{-1}T^{l'}W^{-1}L$.

Let $R = T^h(T^{l'}W^{-1}T^l)^{-1}T^{l'}W^{-1} + K^hW^{-1}(I - T^l(T^{l'}W^{-1}T^l)^{-1}T^{l'}W^{-1})$, we have the equation on each iteration: $H^{(i)} = RL^{(i)}, i = 1, 2, \cdots, \tau$, (note that $L^{(1)} = L$), so that the finally solution $\widehat{H}$ in Algorithm 1 can be written as

$$\widehat{H} = R \sum_{i=1}^{\tau} \alpha_i L^{(i)}. \tag{3.3}$$

Additionally, we can summarize a relation from step 3d of Algorithm 1, that

$$L^{(i)} = L^{(1)} - D \sum_{j=1}^{i-1} H^{(j)}, i = 2, 3, \cdots, \tau. \tag{3.4}$$

We have $H^{(k+1)} = RL^{(k+1)}$ and $L^{(k+1)} = L^{(k)} - DH^{(k)}$ (see step 3d in Algorithm 1) so that

$$H^{(k+1)} = H^{(k)} - RDH^{(k)}, k = 1, 2, \cdots, \tau - 1. \tag{3.5}$$

It is not difficult to get the following derivation from equations (3.3), (3.4) and (3.5),

$$\begin{aligned}
\widehat{H} &= R \sum_{i=1}^{\tau} \alpha_i L^{(i)} \\
&= R\alpha_1 L^{(1)} \\
&+ R\alpha_2 (I - DR) L^{(1)} \\
&+ R\alpha_3 \left((I - DR) - D(I - RD)R \right) L^{(1)} \\
&+ R\alpha_4 \left((I - DR) - D(I - RD)R - D(I - RD)^2 R \right) L^{(1)} \\
&\quad \vdots \\
&+ R\alpha_\tau \left((I - DR) - D(I - RD)R \cdots - D(I - RD)^{\tau - 2} R \right) L^{(1)}, \\
&= R \left(\alpha_1 I + \alpha_2 (I - DR) + \sum_{i=3}^{\tau} \alpha_i ((I - DR) - \sum_{j=1}^{i-2} D(I - RD)^j R) \right) L^{(1)}, \\
&= \left(\sum_{i=1}^{\tau} \alpha_i R - \sum_{i=2}^{\tau} \alpha_i RDR - \alpha_i \sum_{i=3}^{\tau} \sum_{j=1}^{i-2} RD(I - RD)^j R \right) L^{(1)}.
\end{aligned} \tag{3.6}$$

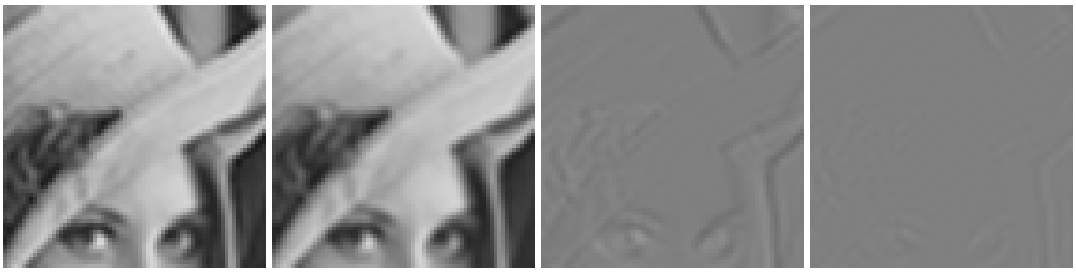

(a) $\widehat{H}$ (b) $H^{(1)}$ (c) $H^{(2)}$ (d) $H^{(3)}$

FIG. 2. *Super-resolution image 'lena' by Algorithm 1; (a) is the sum image of $H^{(i)}, i = 1, 2, 3$; (b) is the computed image for first iteration. For better vision, we add 0.5 to the intensities of $H^{(2)}$ and $H^{(3)}$ to obtain (c) and (d), respectively. From last two images, we know that $H^{(2)}$ and $H^{(3)}$ pick up some image details.*

□

This is the closed-form expression of image super-resolution via the proposed iterative RKHS method. Note that, D, a down-sampling operator from fine grids to coarse grids, is not an explicit matrix sometimes, but it is easy to be implemented. For instance, if the down-sampling approach is bicubic interpolation, we only need to use MATLAB command 'imresize' to image on the fine grid.

COROLLARY 3.2. *In our experiments, we set $\tau = 3$, $\alpha_1 = \alpha_2 = \alpha_3 = 1$. By Theorem 3.1, the finally closed-form solution can be computed by*

$$\widehat{H} = (3R - 3RDR + RDRDR)\, L, \tag{3.7}$$

with R, L and D described in Theorem 3.1.

Remark 4 *For blur case, we only need to replace D with DB in Theorem 3.1 where B is a blurring operator, and get similar conclusions as in Theorem 3.1 and Corollary 3.2.*

In what follows, we will compare the proposed approach with some competitive methods.

4. Numerical experiments. In this section, we compare the proposed approach with nearest-neighbor interpolation, bicubic interpolation and two state-of-the-art learning-based methods [56, 58].

We use two kinds of test images. One is low-resolution images without high-resolution ground-truth images (see Section 4.1). One is simulated low-resolution images from known high-resolution images (see Section 4.2). In the later case, one has high-resolution ground-truth available for quantitative comparisons. Additionally, we divide Section 4.2 into three cases: blur-free (see example 4), Gaussian blur (see example 5) and Gaussian noise (see example 6). All experiments are done in MATLAB(R2013a) on a computer of 16Gb RAM and Intel(R) Core(TM) i7-3820 CPU: @3.60 GHz, 3.60 GHz.

The proposed Algorithm 1 is for gray-scale images. To deal with color image super-resolution, we apply Algorithm 1 to each channel. Peak signal-to-noise ration (PSNR) for color images is defined as

$$\mathrm{PSNR} = 10 \cdot \log_{10}\left(\frac{3mn \cdot \mathrm{Peak}_G^2}{\|\vec{G} - \vec{H}\|_2^2}\right), \tag{4.1}$$

where Peak_G is the maximum possible intensity of image [1], $\vec{G}$ and $\vec{H}$ are vector forms of ground-truth image $G \in \mathbb{R}^{m\times n\times 3}$ and computed image $H \in \mathbb{R}^{m\times n\times 3}$, respectively.

A remark on parameter selection: The related parameters in Algorithm 1 are easy to select. We set $\lambda = 10^{-35}$ for all noise-free case. For noise case, λ increases as the noise level increases. We set maximum iteration to be 3, and coefficients $\alpha_1 = 1$, $\alpha_2 = 1$, $\alpha_3 = 1$ for all experiments. Additionally, we set $M = 6$ so that $\phi_1(t) = 1, \phi_2(t) = x, \phi_3(t) = y, \phi_4(t) = xy$, $\phi_5(t) = x^2, \phi_6(t) = y^2$ (see details in Section 2.3).

[1] http://en.wikipedia.org/wiki/Peak_signal-to-noise_ratio

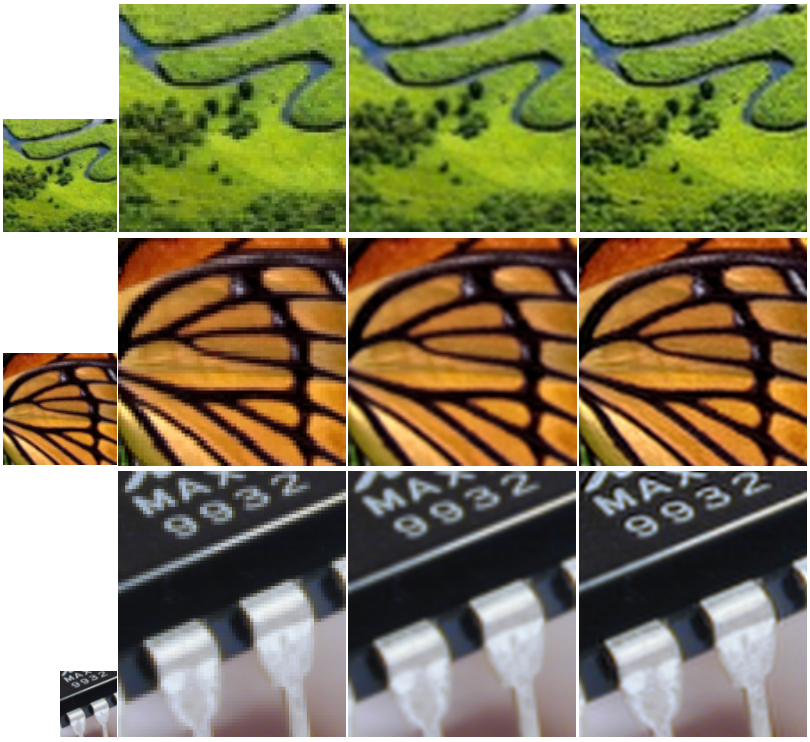

FIG. 3. ***Visual results for example 1.*** *Compare the proposed method with two classical super-resolution methods: nearest-neighbor interpolation and bicubic interpolation. The test images are three natural images captured online, i.e., 'landscape' (first row: low-resolution size* 64×64*, upscaling factor: 2), 'butterflywing' (second row:* 64×64*, upscaling factor: 133/64), and 'text' (third row:* 74×64*, upscaling factor: 4). First column: low-resolution inputs; Second to fourth columns: super-resolution results of nearest-neighbor interpolation, bicubic interpolation and the proposed method. Jaggy and blur artifacts are observed in nearest-neighbor interpolation (second column) and bicubic interpolation (third column), respectively. The proposed SR-RKHS performs best visually (color images are better visualized in the pdf file).*

4.1. Results on low-resolution natural images without ground-truth. In this section, experiments are based on natural images without ground-truth, so quantitative comparisons (e.g., PSNR) will not be done.

Example 1: Compare with nearest-neighbor and bicubic interpolation methods. In this section, three natural images, 'landscape', 'butterflywing' and 'text', are used. Low-resolution images with different sizes and upscaling factors have been tested. In Figure 3, we compare the proposed SR-RKHS method with two interpolation methods: nearest-neighbor interpolation and bicubic interpolation. The three test images have different upscaling factors: 2, 133/64 and 4. Resulted images by nearest-neighbor interpolation and bicubic interpolation generate jaggy effect and blur effect, respectively, whereas SR-RKHS performs best.

Example 2: Compare with a state-of-the-art learning-based method. We compare the proposed SR-RKHS method with a state-of-the-art learning-based method by Yang et. al [56]. In Figure 4, a natural image, 'babyface' with size 64×64, has been tested with upscaling factor 3. As shown in Figure 4, super-resolution images, obtained by nearest-neighbor and bicubic interpolation methods, show somewhat jaggy and blur effect, respectively. Contrastively, the last two images in Figure 4, generated by the learning-based method and the proposed SR-RKHS method, respectively, preserve details well. The visual comparison demonstrates that the two methods are comparable approaches. However, note that the learning-based method needs a lot of data for learning while the proposed method only uses one low-resolution image.

FIG. 4. ***Visual results for example 2.*** *Compare the proposed method with two classical super-resolution methods and one state-of-the-art learning-based method. From left to right: the low-resolution input 'babyface' with size* 64×64*, results of nearest-neighbor interpolation, bicubic interpolation, learning-based approach by Yang et al. [56] and the proposed method. The upscaling factor is 3. The proposed method (last one) is better than nearest-neighbor and bicubic interpolation methods, and is comparable with the learning-based method.*

FIG. 5. ***Visual results for example 3.*** *Compare the proposed method, using different down-sampling approaches, with two interpolation methods. First column: low-resolution input 'lena'; Second to fifth columns: super-resolution results of nearest-neighbor interpolation, bicubic interpolation, the proposed method using bicubic interpolation down-sampling (SR-RKHS) and the proposed method using 'dyaddwon' down-sampling (SR-RKHSdy). Upscaling factor is 2. Jaggy and blur artifacts are observed in nearest-neighbor interpolation (second column) and bicubic interpolation (third column), respectively. The proposed SR-RKHSdy method performs better than the proposed SR-RKHS method.*

Example 3: The proposed method with different down-sampling operators D. In the above two examples, we used bicubic interpolation as down-sampling operator D (see step 3c of Algorithm 1). In this section, we will take a different down-sampling method. We denote the different down-sampling method as 'dyaddown' that means keeping every other one row and column for high-resolution image. In Figure 5, we compare the proposed method, using the mentioned down-sampling approaches, with nearest-neighbor interpolation and bicubic interpolation. The proposed method with 'dyaddown' down-sampling, denoted as SR-RKHSdy, performs best. Especially, it is better than the proposed method with bicubic interpolation down-sampling, denoted as SR-RKHS (see last two columns in Figure 5). However, 'dyaddown' down-sampling requires the high-resolution image should be 2^j $(j = 1, 2, \cdots)$ times the size of the low-resolution image. This makes 'dyaddown' down-sampling very limited. So we will not use 'dyaddown' down-sampling in the following experiments.

4.2. Results on low-resolution images simulated from known ground-truth images. To provide quantitative comparisons in terms of PSNR, we start from some high-resolution images, treat them as ground-truth and simulate low-resolution images according to equation (1.1). We divide the experiments of this section into three cases: i) blur-free (example 4); ii) Gaussian blur (example 5); iii) Gaussian noise (example 6). For these cases, we compare the proposed method with nearest-neighbor interpolation, bicubic interpolation, one learning-based method by Yang et al. [56] and another learning-based method by Zeyde et al. [58].

TABLE 1

***PSNR(dB) for blur-free case**: first to seventh examples: 'purplebutterfly' (size from 90×90 to 160×160), 'text' (90×90 to 150×150), 'babyface' (80×80 to 200×200), 'lena' (40×40 to 80×80), 'sar' (85×85 to 180×180),'landscape' (45×45 to 84×84) and 'butterflywing' (45×45 to 100×100); eighth two ninth examples: 'babyface' (80×80 to 240×240) and 'dog' (70×70 to 210×210); last two examples: 'babyface' (80×80 to 234×234 with shaving boundary) and 'comic' (80×50 to 234×144 with shaving boundary). The proposed SR-RKHS method outperforms nearest-neighbor and bicubic interpolation methods, while performs similarly with that of Yang et al. [56] and Zeyde et al. [58].*

Test image	Nearest-neighbor	Bicubic	SR-RKHS
purplebutterfly	22.83	25.55	26.74
text	27.07	31.34	33.70
babyface	29.81	31.19	31.51
lena	28.10	32.23	34.20
sar	19.48	22.42	23.96
landscape	25.01	27.01	27.91
butterflywing	23.93	28.30	29.27
	Bicubic	Yang et al. [56]	SR-RKHS
babyface	29.85	29.99	30.00
dog	38.93	39.34	39.63
	Yang et al. [56]	Zeyde et al. [58]	SR-RKHS
babyface	30.01	30.31	30.08
comic	21.70	21.80	21.24

Example 4: Results for blur-free case. In the section, we compare the proposed method with nearest-neighbor and bicubic interpolation methods, and two state-of-the-art learning-based methods. Visual and quantitative results are shown in Figure 6, Figure 7, Figure 8 and Table 1. In Figure 6, the proposed SR-RKHS method (forth column) overcomes jaggy effect of nearest-neighbor interpolation (second column) and reduces blur effect of bicubic interpolation significantly (third column). Note that the proposed method can be applied to any upscaling factors, including fractional factors, e.g., 16/9 for 'purplebutterfly' and 5/2 for 'babyface'. Whereas sometimes this is not true for other methods, such as [2]. In Figure 7, we compare the proposed method with a state-of-the-art learning-based method by Yang et al. [56]. In Figure 8, another state-of-the-art method by Zeyde et al. [58] is also employed to compare with the proposed method. The resulted super-resolution images by the proposed method and the two learning-based methods are similar. In Table 1, quantitative results of more test images, e.g., 'lena', 'sar', 'landscape' and 'butterflywing', can be found. From Table 1, the proposed method gets higher PSNR than bicubic interpolation, and similar PSNR with the two learning-based methods in [56, 58]. In particular, we have to note that the method in [58] shaves boundary pixels of resulted super-resolution images. For instance, if we set upscaling factor 3 for a 80×80 low-resolution image, the resulted image should be 240×240. However, the method in [58] shaves 3 pixels on the boundary to get 234×234 super-resolution image. From Figure 7 and Figure 8, we know that the proposed method is comparable with the both learning-based methods.

Example 5: Results for Gaussian blur case. In this section, four test images, synthetic aperture radar (SAR) image 'sar', natural images 'babyface', 'dog' and 'pepper', have been employed. Different Gaussian blur are added to ground-truth images manually, then we get blurred low-resolution images according to equation (1.1) with bicubic interpolation down-

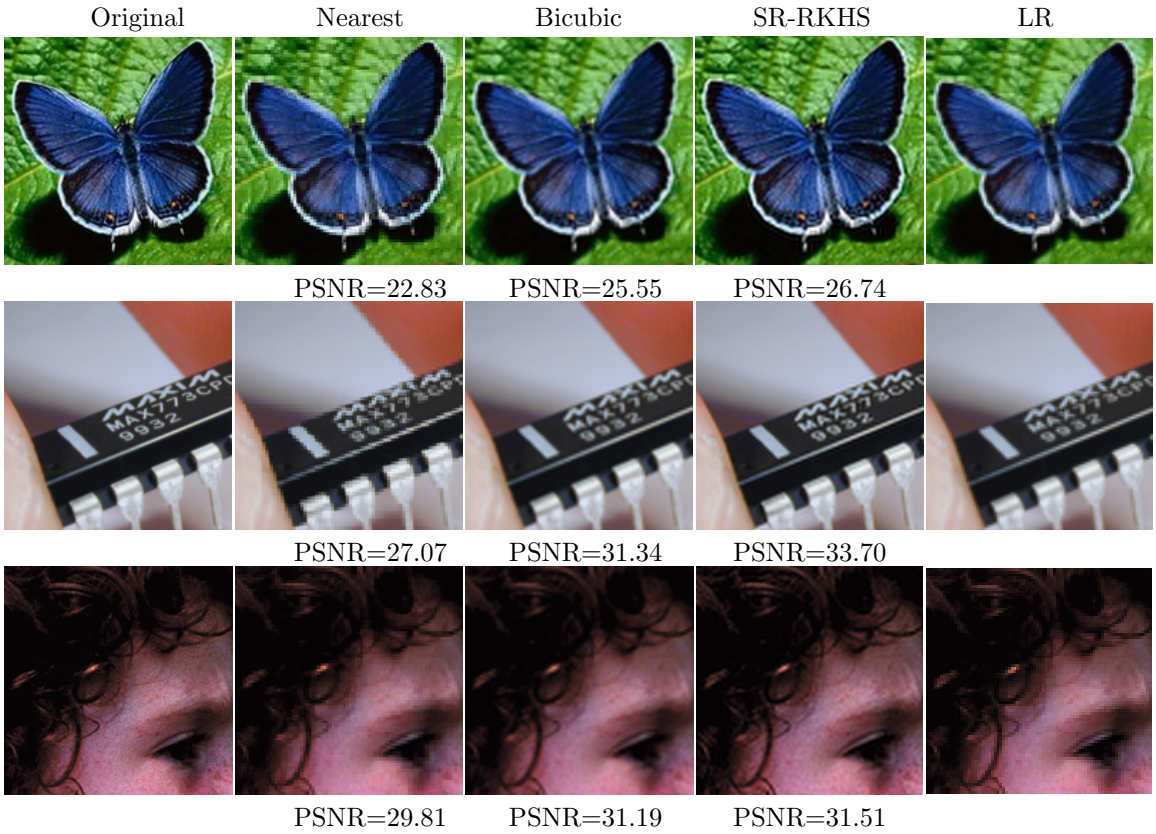

FIG. 6. ***Visual results for blur-free case (see example 4).*** *Compare the proposed method with two interpolation methods for blur-free case. Test images: 'purplebutterfly' from size* 90×90 *to* 160×160 *(first row), 'text' from* 90×90 *to* 150×150 *(second row), 'babyface' from* 80×80 *to* 200×200 *(third row); The low-resolution images are simulated from known ground-truth images according to equation (1.1). First column: ground-truth images; Second to fourth columns: results of nearest-neighbor interpolation, bicubic interpolation and the proposed SR-RKHS method; The last column: low-resolution images (denoted as 'LR'). Note that, the proposed method can be applied to any upscaling factors, including fractional factors, e.g., 16/9 for 'purplebutterfly' and 5/3 for 'text'.*

sampling.

We compare the proposed SR-RKHS method with bicubic interpolation and two state-of-the-art learning-based methods by Yang et al. [56] and Zeyde et al. [58]. In Figure 9 and Figure 10, the learning-based methods and the proposed SR-RKHS method, both better than bicubic interpolation, do not show significantly visual disparity. Additionally, PSNR shown in Table 2 can not distinguish which method preforms significantly absolutely. Thus we regard the proposed SR-RKHS method and the learning-based methods as three comparable and competitive methods. The learning-based methods, however, need to train a lot of data to generate a new dictionary when every time the upscaling factor changes. Furthermore, they are not completely single image super-resolution as two large sets of low-resolution and high-resolution images are required for learning. In comparison, the proposed non-learning SR-RKHS method, only requiring one low-resolution image as an input, has a simple closed-form expression and competitive performance, both visually and quantitatively.

Example 6: Results for noise case. We also compare the proposed method with bicubic interpolation and two state-of-the-art learning-based methods by Yang et al. [56] and Zeyde et al. [58], with noisy low-resolution images as inputs. We add 3%, 2% and 3% Gaussian white noise to the ground-truth images 'sar', 'babyface' and 'landscape', respectively, then get noisy low-resolution images by bicubic interpolation down-sampling (slightly different with equation (1.1)). In Figure 11, the proposed method gets better visual results than bicubic

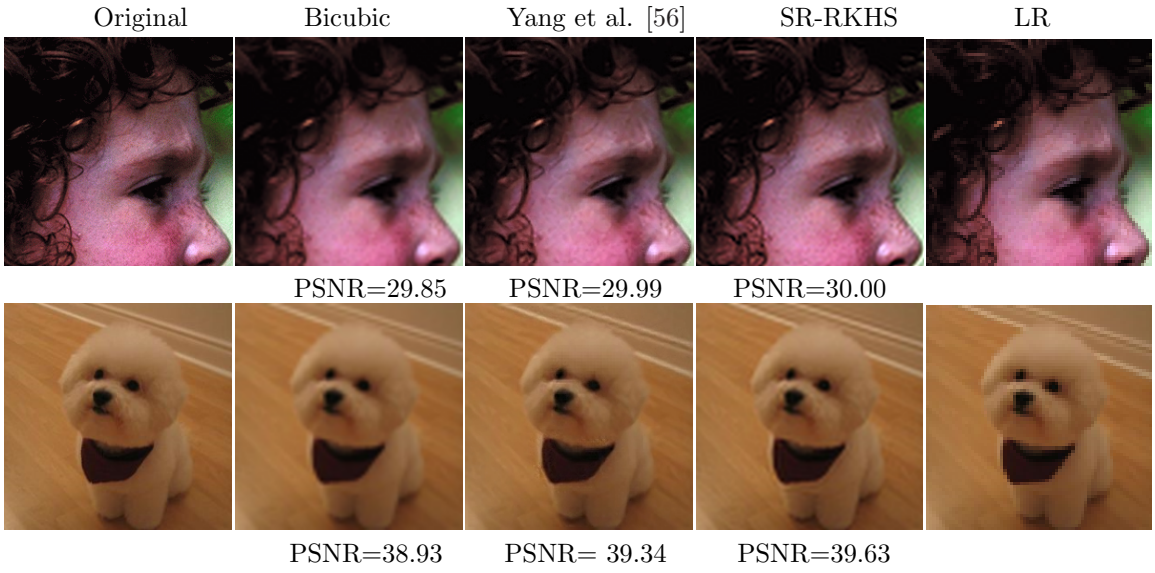

FIG. 7. ***Visual results for blur-free case (see example 4).*** *Compare the proposed method with bicubic interpolation method and the learning-based method by Yang et al.[56]. Test images: 'babyface' from size* 80×80 *to* 240×240 *(first row), 'dog' from* 70×70 *to* 210×210 *(second row). Third column: results of the learning-based method [56].*

TABLE 2
PSNR(dB) for Gaussian blur case and Gaussian noise case*; 'sd' means the standard derivation, 'Noise' means the level of Gaussian noise.*

Test image(**Blur case**)	Bicubic	Yang et al. [56]	SR-RKHS
sar(sd:2)	18.59	19.48	19.50
babyface(sd:1.5)	29.13	29.38	29.92
dog(sd:2.5)	38.20	38.59	39.48
dog(sd:1)	38.45	38.83	39.98
	Yang et al. [56]	Zeyde et al. [58]	SR-RKHS
pepper(sd:1)	29.28	29.52	29.51
Test image(**Noise case**)	Bicubic	Yang et al. [56]	SR-RKHS
sar(Noise:3%)	19.15	19.47	19.50
babyface(Noise:2%)	30.84	30.88	30.95
	Yang et al. [56]	Zeyde et al. [58]	SR-RKHS
landscape(Noise:3%)	24.40	24.58	24.21

interpolation method, and obtains comparable visual results with the learning-based method in [56]. In Figure 12, it demonstrates that the proposed method and the two learning-based are comparable approaches visually. From Table 2, we know that PSNR of the proposed method and the two learning-based methods are comparable, and all higher than bicubic interpolation.

5. Conclusions. Given a low-resolution image, the super-resolution problem was casted as an image intensity function estimation problem. We assumed the underlying intensity function, defined on a continuous domain, belongs to a 2D thin-plate spline based RKHS. The basis coefficients of the space were computed using the low-resolution image. To recover sharp high-resolution images with details, we proposed an iterative RKHS method. The intensity function

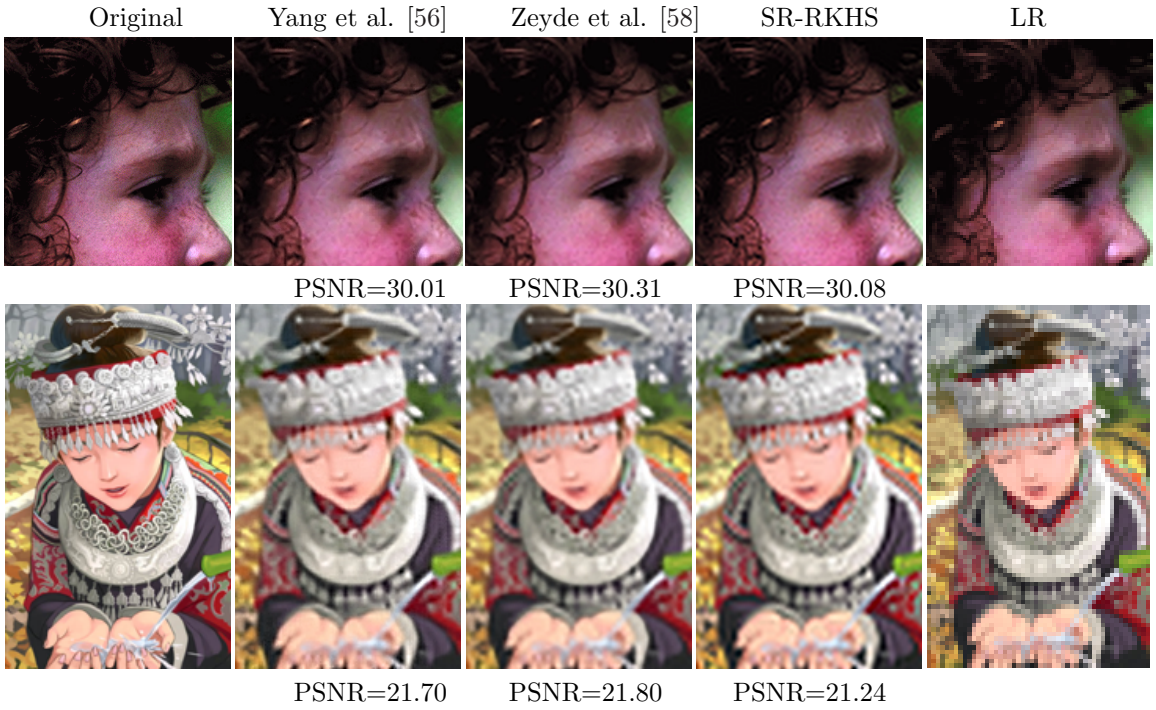

FIG. 8. ***Visual results for blur-free case (see the example 4).*** *Compare the proposed method with bicubic interpolation method and two learning-based methods. Test images: 'babyface' from size* 80×80 *to* 234×234 *with shaving boundary (see details on shaving boundary in example 4) (first row), 'comic' from* 80×50 *to* 234×144 *with shaving boundary (second row). Third column: results of the learning-based method [58].*

could then be estimated at any fine grids to get high-resolution image with any upscaling factors. Moreover, a closed-form solution for the iterative RKHS method is also given in this paper. Many quantitative and qualitative experiments in various cases (blur-free, blur and noise) show that the proposed approach outperforms two classical single image super-resolution methods: nearest-neighbor interpolation and bicubic interpolation. It is also comparable with two state-of-the-art learning-based methods which need a lot of data for learning.

Acknowledgement. The first and third authors thank the support by 973 Program (2013CB329404), NSFC (61370147), Sichuan Province Sci. & Tech. Research Project (2012GZX 0080). The first author is also supported by Fundamental Research Funds for the Central Universities (A03009023401040) and Outstanding Doctoral Students Academic Support Program of UESTC (A1098524023901001044).

REFERENCES

[1] C. B. Atkins, C. A. Bouman, and J. P. Allebach. Tree-based resolution synthesis. *International Conference on Image Processing (ICIP)*, pages 405–410, 1999.

[2] C. B. Atkins, C. A. Bouman, and J. P. Allebach. Optimal image scaling using pixel classification. *International Conference on Image Processing (ICIP)*, pages 864–867, 2001.

[3] S. Borman and R. L. Stevenson. Super-resolution from image sequences - a review. *Midwest Symposium on Circuits and Systems*, pages 374–378, 1998.

[4] P. Bouboulis, K. Slavakis, and S. Theodoridis. Adaptive kernel-based image denoising employing semi-parametric regularization. *IEEE Transactions on Image Processing*, 19:1465–1479, 2010.

[5] E. Candès and C. Fernandez-Granda. Towards a mathematical theory of super-resolution. *To appear in Communications on Pure and Applied Mathematics.*

[6] D. Capel and A. Zisserman. Super-resolution enhancement of text image sequences. *International Conference on Pattern Recognition (ICPR)*, 1:600–605, 2000.

[7] A. Caponnetto, M. Pontil, C. Micchelli, and Y. Ying. Universal multi-task kernels. *Journal of Machine Learning Research (JMLR)*, 9:1615–1646, 2008.

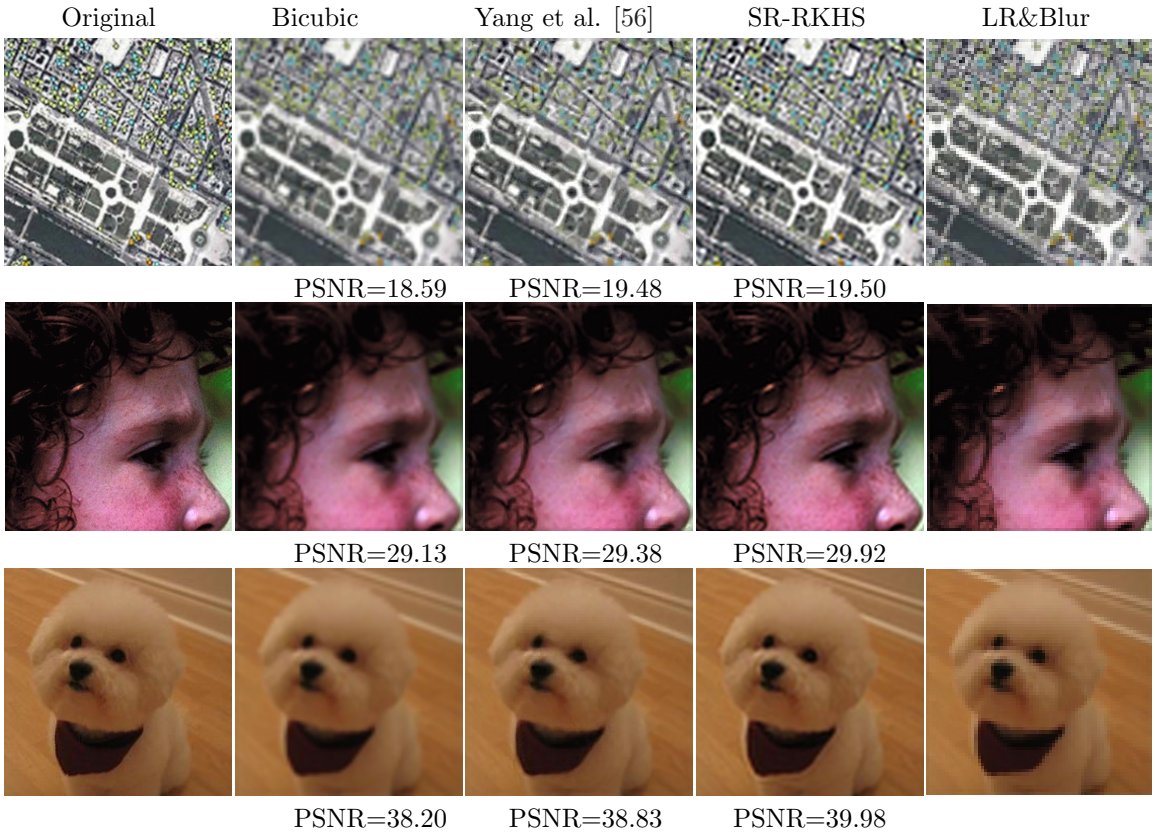

FIG. 9. ***Visual results for Gaussian blur case (see example 5).*** *Compare the proposed method with bicubic interpolation method and one learning-based method by Yang et al. [56]. Blurred low-resolution images: 'sar' with size* 75×75 *(first row), 'babyface' with* 80×80 *(second row) and 'dog' with* 70×70 *(third row); The last column: blurred low-resolution images simulated according to equation (1.1) which blurring operators B are with standard derivations: 2, 1.5 and 1, respectively. The upscaling factors are all 3.*

FIG. 10. ***Visual results for Gaussian blur case (see example 5).*** *Compare the proposed method with two learning-based methods by Yang et al. [56] and Zeyde et al. [58] for Gaussian blur case (standard derivation: 1). Test image: 'pepper' from size* 60×80 *to* 174×234 *with shaving boundary.*

[8] C. Carmeli, E. De Vito, and A. Toigo. Vector valued reproducing kernel Hilbert spaces of integrable functions and Mercer theorem. *Analysis and Applications*, 4:377–408, 2006.

[9] H. Chang, D. Yeung, and Y. Xiong. Super-Resolution through neighbor embedding. *Computer Vision and Pattern Recognition (CVPR)*, 1, 2004.

[10] P. Chatterjee, S. Mukherjee, S. Chaudhuri, and G. Seetharaman. Application of Papoulis-Gerchberg method in image super-resolution and inpainting. *The Computer Journal*, 52:80–89, 2007.

[11] R. R. Coifman and S. Lafon. Geometric harmonics: a novel tool for multiscale out-of-sample extension of empirical functions. *Applied and Computational Harmonic Analysis*, 21:31–52, 2006.

[12] F. Cucker and S. Smale. On the mathematical foundations of learning. *Bulletin of the American Mathematical Society*, 39:1–49, 2002.

[13] G. Daniel, S. Bagon, and M. Irani. Super-Resolution from a single image. *ICCV*, pages 349–356, 2009.

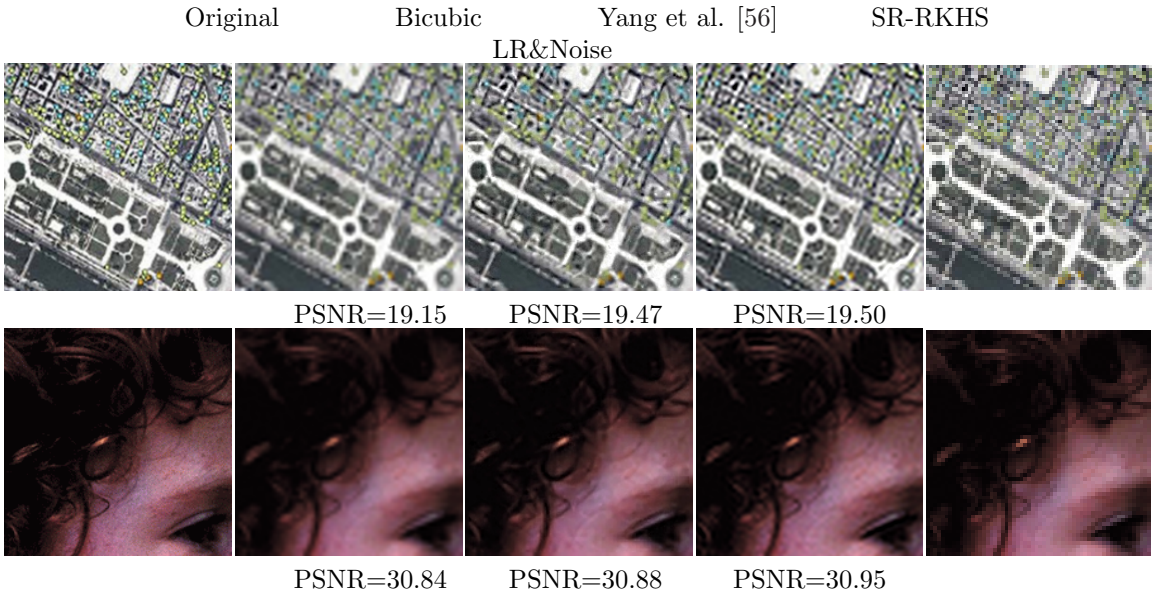

FIG. 11. ***Visual results of images with Gaussian noise (see example 6).*** *Compare the proposed method with bicubic interpolation and the learning-based method by Yang et al. [56]. Noisy and low-resolution images: 'sar' with size* 70×70 *and 'babyface' with* 60×60*; both regularization parameters* $\lambda = 10^{-19}$*. The last column: noisy low-resolution images. The upscaling factors are all 3.*

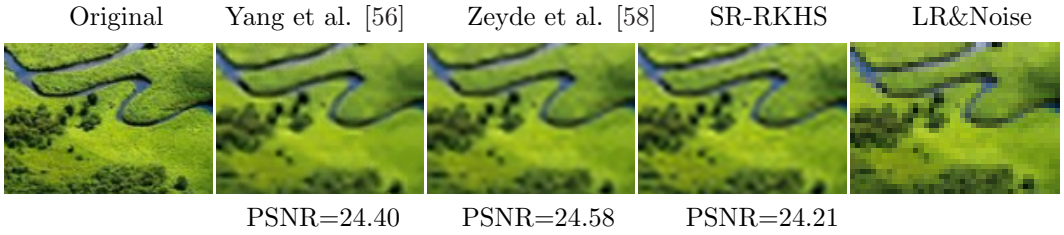

FIG. 12. ***Visual results for Gaussian noise (see example 6).*** *Compare the proposed method with two state-of-the-art learning-based methods by Yang et al. [56] and Zeyde et al. [58] for Gaussian noise case. Test image: 'landscape' from size* 30×40 *to* 84×114 *with shaving boundary (see details on shaving boundary in example 4); The regularization parameter* $\lambda = 10^{-20}$*; First column: ground-truth image; Second to fourth columns: results of Yang et al. method [56], Zeyde et al. method [58] and the proposed SR-RKHS method; last column: noisy low-resolution image.*

[14] W. Dong, G. Shi, L. Zhang, and X. Wu. Superresolution with nonlocal regularized sparse representation. *Proceeding of SPIE*, 2010.

[15] J. Duchon. Fonctions splines et vecteurs aleatoires. *Tech. Report 213, Seminaired Analyse Numerique, Universite Scientifique et Medicale, Grenoble*, 1975.

[16] J. Duchon. Fonctions-spline et esperances conditionnelles de champs gaussiens. *Ann. Sci. Univ. Clermont Ferrand II Math*, pages 19–27, 1976.

[17] J. Duchon. Splines minimizing rotation-invariant semi-norms in Sobolev spaces. *Constructive Theory of Functions of Several Variables*, pages 85–100, 1977.

[18] S. Farsiu, M. D. Robinson, M. Elad, and P. Milanfar. Fast and robust multiframe super resolution. *IEEE transactions on image processing*, 13:1327–1344, 2004.

[19] R. Fattal. Image upsampling via imposed edge statistics. *ACM Transactions on Graphics*, 26, 2007.

[20] C. Fernandez-Granda and E. Candès. Super-resolution via transform-invariant group-sparse regularization. *ICCV*, 2013.

[21] G. Freedman and R. Fattal. Image and video upscaling from local self-examples. *ACM Trans. on Graphics (TOG)*, 30, 2011.

[22] W. T. Freeman, T. R. Jones, and E. C. Pasztor. Example-based super-resolution. *IEEE Computer Graphics and Applications*, 22:56–65, 2002.

[23] W. T. Freeman and E. C. Pasztor. Markov networks for super-resolution. *Proceedings of 34th Annual Conference on Information Sciences and Systems*, 2000.

[24] W. T. Freeman, E. C. Pasztor, and O. T. Carmichael. Learning low-level vision. *International Journal of Computer Vision*, 40:25–47, 2000.

[25] E. Gur and Z. Zalevsky. Single-Image digital super-resolution a revised Gerchberg-Papoulis algorithm. *IAENG International Journal of Computer Science*, 34:251–255, 2007.

[26] L. He, H. Qi, and R. Zaretzki. Beta process joint dictionary learning for coupled feature spaces with application to single image super-resolution. *CVPR*, pages 345–352, 2013.

[27] M. Irani and S. Peleg. Super resolution from image sequence. *Proceedings of 10th International Conference on Pattern Recognition (ICPR)*, pages 115–120, 1990.

[28] S. H. Kang, B. Shafei, and G. Steidl. Supervised and Transductive Multi-Class Segmentation Using p-Laplacians and RKHS methods. *Preprint at uni-kl.de*, 2012.

[29] C. Kim, K. Choi, K. Hwang, and J. B. Ra. Learning-based super-resolution using a multi-resolution wavelet approach. *Iternational workshop on Advance Image Technology (IWAIT)*, 2009.

[30] C. Kim, K. Choi, and J. B. Ra. Improvement on learning-based super-resolution by adopting residual information and patch reliability. *IEEE International Conference on Image Processing (ICIP)*, pages 1197–1200, 2009.

[31] K. Komatsu, T. Igarashi, and T. Saito. Very high resolution imaging scheme with multiple different-aperture cameras. *Signal Processing: Image Communication*, 5:511–526, 1993.

[32] Liyakathunisa and V. K. Ananthashayana. Super resolution blind reconstruction of low resolution images using wavelets based fusion. *International Journal of Computer and Information Engineering*, 2:106–110, 2008.

[33] J. Meinguet. Multivariate interpolation at arbitrary points made simple. *Journal of Applied Mathematics and Physics (ZAMP)*, 30:292–304, 1979.

[34] J. Mercer. Functions of positive and negative type, and their connection with the theory of integral equations. *Philosophical transactions of the royal society of London. Series A, containing papers of a mathematical or physical character*, 209:415–446, 1909.

[35] C. A. Micchelli and M. Pontil. On leaning vector-valued functions. *Neural Computation*, 17:177–204, 2005.

[36] A. Nosedal-Sanchez, C. B. Storlie, T. C. M. Lee, and R. Christensen. Reproducing kernel Hilbert spaces for penalized regression: a tutorial. *The American Statistician*, 66:50–60, 2012.

[37] S. Osher, M. Burger, D. Goldfarb, J. Xu, and W. Yin. An iterative regularization method for total variation-based image restoration. *Multiscale Modeling and Simulation*, 4:460–489, 2005.

[38] S. C. Park, M. K. Park, and M. G. Kang. Super-Resolution image reconstruction: a technical overview. *IEEE signal processing magazine*, 20:21–36, 2003.

[39] M. H. Quang, S. H. Kang, and T. M. Le. Image and video colorization using vector-valued reproducing kernel Hilbert spaces. *Journal of Mathematical Imaging and Vision*, 37:49–65, 2010.

[40] B. Schökopf and A. Smola. Learning with kernels: support vector machines, regularization, optimization, and beyond. *MIT Press, Cambridge*, 2002.

[41] R. Seaman and M. Hutchinson. Compamtive real data tests of some objective analysis methods by withholding. *Australian Meteorological Magazine*, 33:37–46, 1985.

[42] A. J. Shah and S. B. Gupta. Image super resolution - a survey. *International Conference on Emerging Technology Trends in Electronics, Communication and Networking*, 2012.

[43] J. Shawe-Taylor and N. Cristianini. Kernel methods for pattern analysis. *Cambridge University Press, Cambridge*, 2004.

[44] J. Sun, J. Sun, Z. Xu, and H.-Y. Shum. Image super-resolution using gradient profile prior. *CVPR*, pages 1–8, 2008.

[45] J. Sun, N. N. Zheng, H. Tao, and H. Shum. Image hallucination with primal sketch priors. *IEEE Conference on Computer Vision and Pattern Recognition (CVPR)*, 2:729–736, 2003.

[46] S.-C. Tai, T.-M. Kuo, C.-H. Iao, and T.-W. Liao. A fast algorithm for single-image super resolution in both wavelet and spatial domain. *International Symposium on Computer, Consumer and Control*, pages 702–705, 2012.

[47] Y.-W. Tai, S. Liu, M. Brown, and S. Lin. Super resolution using edge prior and single image detail synthesis. *CVPR*, pages 2400–2407, 2010.

[48] H. Takeda, S. Farsiu, and P. Milanfar. Kernel regression for image processing and reconstruction. *IEEE Transactions on Image Processing*, 16:349–366, 2007.

[49] M. F. Tappen, B. C. Russell, and W. T. Freeman. Exploiting the sparse derivative prior for super-resolution and image demosaicing. *IEEE Workshop on Statistical and Computational Theories of Vision*, 2003.

[50] J. D. Van Ouwerkerk. Image super-resolution survey. *Image and Vision Computing*, 24:1039–1052, 2006.

[51] F. Viola, A. W. Fitzgibbon, and R. Cipolla. A unifying resolution-independent formulation for early vision. *CVPR*, pages 494–501, 2012.

[52] G. Wahba. Spline models for observational data. *SIAM. CBMS-NSF Regional Conference Series in Applied Mathematics*, 59, 1990.

[53] G. Wahba and J. Wendelberger. Some new mathematical methods for variational objective analysis using splines and cross-validation. *Monthly Weather Review*, 108:1122–1145, 1980.

[54] Q. Xie, H. Chen, and H. Cao. Improved example-based single-image superresolution. *International Congress on Image and Signal Processing (CISP)*, 3:1204–1207, 2010.

[55] J. Yang, Z. Wang, L. Zhe, and T. Huang. Coupled dictionary training for image super-resolution. *IEEE transactions on image processing*, 21:3467–3478, 2011.

[56] J. Yang, J. Wright, T. Huang, and Y. Ma. Image super-resolution via sparse representation. *IEEE transactions on image processing*, 19:2861–1873, 2010.

[57] J. Yang, J. Wright, Y. Ma, and T. Huang. Image super-resolution as sparse representation of raw image patches. *IEEE Conference on Computer Vision and Pattern Recongnition (CVPR)*, pages 1–8, 2008.

[58] R. Zeyde, M. Elad, and M. Protter. On single image scale-up using sparse-representations. *Curves and Surfaces, Lecture Notes in Computer Science*, 6920:711–730, 2012.

[59] Y. Zhao, J. Yang, Q. Zhang, S. Lin, Y. Cheng, and Q. Pan. Hyperspectral imagery superresolution by sparse representation and spectral regularization. *EURASIP Journal on Advances in Signal Processing*, 2011.

[60] H. Zheng, A. Bouzerdoum, and S. L. Phung. Wavelet based nonlocalmeans superresolution for video sequences. *IEEE International Conference on Image Processing (ICIP)*, pages 2817–2820, 2010.